Available online at www.sciencedirect.com
ScienceDirect
Journal of Power Sources 177 (2008) 369–375
JOURNAL OF POWER SOURCES
www.elsevier.com/locate/jpowsour

# Theoretical analysis of reversible solid oxide fuel cell based on proton-conducting electrolyte

Meng Ni, Michael K.H. Leung *, Dennis Y.C. Leung

*Department of Mechanical Engineering, The University of Hong Kong, Pokfulam Road, Hong Kong, China*

Received 5 October 2007; received in revised form 19 November 2007; accepted 19 November 2007
Available online 23 November 2007

**Abstract**

A single reversible solid oxide fuel cell (RSOFC) can accomplish two functions: (1) as a solid oxide steam electrolyzer (SOSE) for hydrogen production and (2) as a solid oxide fuel cell (SOFC) for power generation. An electrochemical model was developed to study the performance of an RSOFC based on a proton-conducting electrolyte (RSOFC-H). In both SOSE and SOFC modes, the hydrogen electrode-supported configuration was identified as the most favorable design to achieve high energy conversion efficiency of RSOFC-H. For comparison, in a previous study on conventional RSOFC based on an oxygen ion-conducting electrolyte (RSOFC-O), the hydrogen electrode-supported configuration was found to be favorable in the SOFC mode but such configuration would cause high concentration overpotential in the SOSE mode. Thus, the oxygen electrode-supported configuration was desirable for RSOFC-O operating in the SOSE mode. The results obtained in this study show that RSOFC-H has a natural advantage over RSOFC-O in terms of structural design. The modeling study signifies the difference between RSOFC-H and RSOFC-O and can serve as a useful tool for further design optimization.
© 2007 Elsevier B.V. All rights reserved.

*Keywords:* Solid oxide fuel cell; *J–V* characteristics; Proton-conducting ceramics; Solid oxide steam electrolyzer

## 1. Introduction

A reversible solid oxide fuel cell (RSOFC) can be operated in the SOSE mode to produce hydrogen fuel and the same RSOFC can later consume the hydrogen fuel to generate electricity in the SOFC mode [1–3]. Due to the site-specific and intermittent characteristics of renewable resources, such as solar and wind, hydrogen is a potentially useful energy carrier to support renewable utilization. The capability of performing dual function using a single cell can thus make RSOFC potentially economically sound to better utilize renewable resources.

Several experimental studies on conventional RSOFC based on oxygen ion-conducting electrolyte (RSOFC-O) have been performed to investigate the performance characteristics of RSOFC in both working modes [4–6]. Recently, a modeling study on the concentration overpotentials of an RSOFC-O has been conducted [2]. The transport and reactions involved in the two working modes of the RSOFC-O are illustrated in Fig. 1a and b, respectively. It is found that a hydrogen electrode support is favorable to the SOFC mode while the oxygen electrode support is favorable to the SOSE mode [2]. The difference in the optimal designs is due to the different mass transport characteristics of gaseous species in the porous electrodes in the SOSE and SOFC modes. This study indicates that RSOFC-O has fundamental problems. No matter which electrode support (hydrogen or oxygen) is selected, the RSOFC-O will exhibit high concentration overpotential in one of the two working modes.

Alternatively, an RSOFC can be built with a proton-conducting electrolyte (RSOFC-H). Although some experimental studies have been accomplished to characterize the performance of RSOFC-H in the SOSE mode and SOFC mode [7–10], the present literature lacks detailed modeling analyses on RSOFC-H. Modeling studies are important for better understanding of the working mechanisms as well as for design optimization. Under the same operating conditions (i.e. temperature, current density), an RSOFC-H working in either SOFC or SOSE mode has identical Ohmic overpotentials. In addition, the exchange current densities for SOSE and SOFC are identical. Therefore, the activation overpotentials of SOFC and SOSE can be considered identical as well using the simplified

* Corresponding author. Tel.: +852 2859 2628; fax: +852 2858 5415.
*E-mail address:* mkhleung@hku.hk (M.K.H. Leung).

0378-7753/$ – see front matter © 2007 Elsevier B.V. All rights reserved.
doi:10.1016/j.jpowsour.2007.11.057

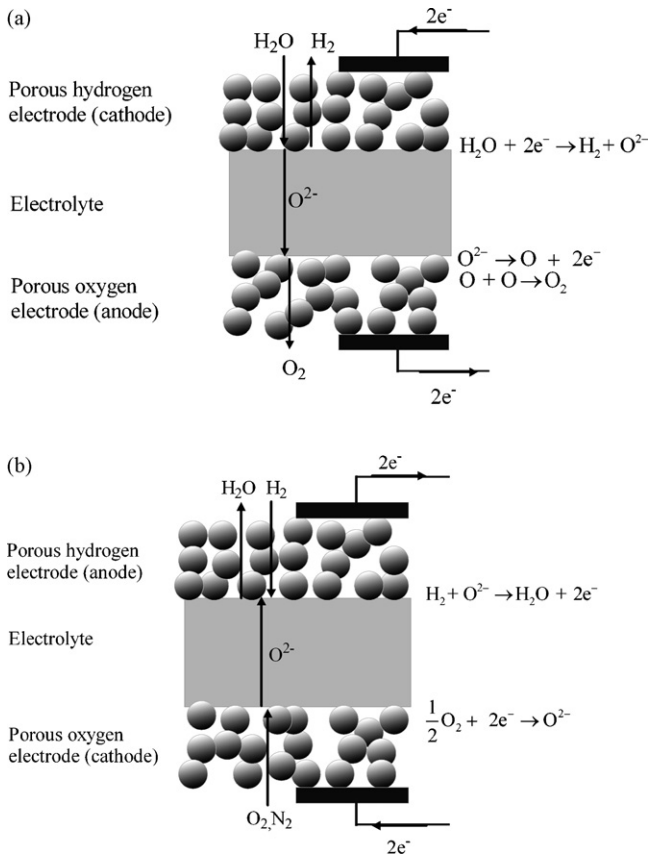


Fig. 1. Working mechanisms of RSOFC-O: (a) SOSE mode and (b) SOFC mode.

Butler-volmer equation (omitting the reactant/product concentrations). It is noted that the activation overpotential is independent of the electrode thickness, which is the focus of the present study. These overpotentials can be calculated with the electrochemical model recently developed [11]. On the other hand, the concentration overpotentials are different between the SOSE mode and the SOFC mode due to different gas transport characteristics in the porous electrodes. Therefore, the concentration overpotentials are the sole factor responsible for different RSOFC-H current–voltage (*J–V*) characteristics between the SOSE and SOFC modes. For this reason, this electrochemical modeling study on RSOFC-H focuses on the concentration overpotentials in both SOSE and SOFC modes.

## 2. Model development

### 2.1. Operating mechanisms

The fundamental working mechanisms of an RSOFC-H working in the SOSE mode are illustrated in Fig. 2a. Steam is fed to the porous oxygen electrode and transported to the interface between the oxygen electrode and the electrolyte where electrochemical reactions take place. The important electrochemical reaction steps include (1) adsorption of steam onto the surface of electrode particles, (2) electrochemically splitting of steam to form oxygen, electrons and protons, (3) desorption of oxygen produced, and (4) incorporation of proton into the electrolyte. The protons are transported through the dense electrolyte to the porous hydrogen electrode where they are combined with electrons to form $H_2$. It should be mentioned that the consumption of $H_2O$ and generation of $O_2$ will result in concentration gradients of these two species in the porous oxygen electrode. In addition, the molar production rate of $O_2$ is only half of the molar consumption rate of $H_2O$, thus, the pressure at the electrode–electrolyte interface is lower than that at the surface of the electrode. Therefore, the transport of $H_2O$ and $O_2$ is by means of both diffusion and permeation. Since $H_2$ is the only gas in the porous hydrogen electrode, it is transported by means of permeation.

The working mechanisms of RSOFC-H in the SOFC mode are illustrated in Fig. 2b. Similar to the SOSE mode, $H_2$ (as a single gas) is transported in the porous hydrogen electrode by means of permeation, while the $O_2$ and $H_2O$ are transported in the porous oxygen electrode by means of both diffusion and permeation.

### 2.2. RSOFC-H cell potentials

In the SOSE mode, the *J–V* characteristics of an RSOFC-H can be expressed as:

$$V^{\mathrm{SOSE}} = E + \eta_{\mathrm{act,H_2}} + \eta_{\mathrm{act,O_2}} + \eta_{\mathrm{Ohm}} + \eta^{\mathrm{SOSE}}_{\mathrm{conc,H_2}} + \eta^{\mathrm{SOSE}}_{\mathrm{conc,O_2}} \quad (1)$$

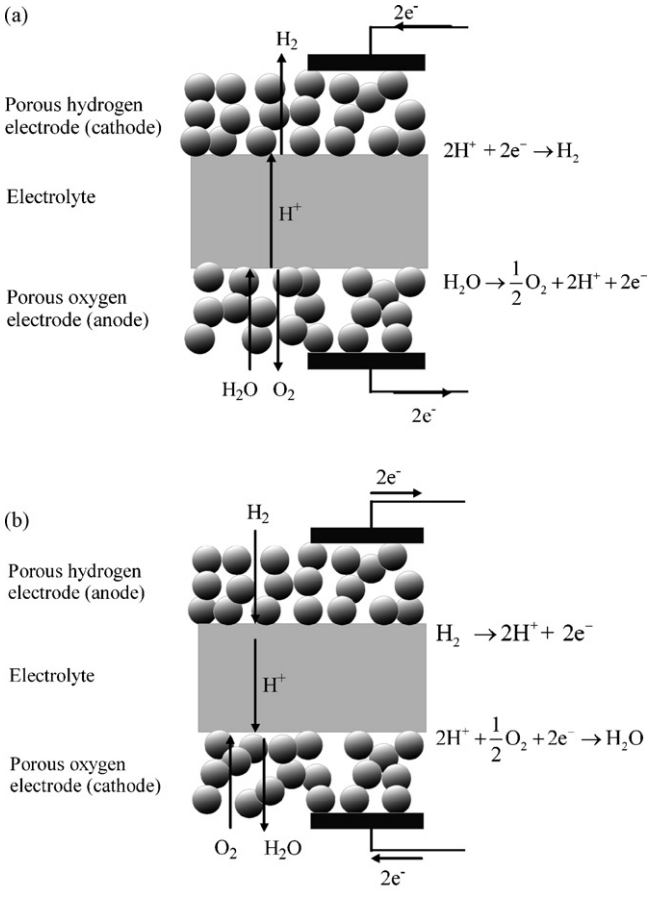


Fig. 2. Working mechanisms of RSOFC-H: (a) SOSE mode and (b) SOFC mode.

where $E$ is the equilibrium potential; $\eta_{act,H_2}$ and $\eta_{act,O_2}$ stand for the activation overpotentials of the hydrogen electrode and oxygen electrode, respectively; $\eta_{Ohm}$ represents the Ohmic overpotential; and $\eta^{SOSE}_{conc,H_2}$ and $\eta^{SOSE}_{conc,O_2}$ are the concentration overpotentials at the hydrogen electrode and oxygen electrode, respectively.

In the SOFC mode, the operating potential ($V^{SOFC}$) of an RSOFC-H can be determined as:

$$V^{SOFC} = E - \eta_{act,H_2} - \eta_{act,O_2} - \eta_{Ohm} - \eta^{SOFC}_{conc,H_2} - \eta^{SOFC}_{conc,O_2} \quad (2)$$

where $\eta^{SOFC}_{conc,H_2}$ and $\eta^{SOFC}_{conc,O_2}$ stand for the concentration overpotentials of the two electrodes working in the SOFC mode.

The equilibrium potential $E$ can be determined with the Nernst equation [12]. The Ohmic ($\eta_{Ohm}$) and activation overpotentials ($\eta_{act,H_2}$ and $\eta_{act,O_2}$) as well as the concentration overpotentials in the SOFC mode ($\eta^{SOSE}_{conc,H_2}$ and $\eta^{SOSE}_{conc,O_2}$) can be determined with an electrochemical model recently developed [11]. The concentration overpotentials in the SOSE mode ($\eta^{SOFC}_{conc,H_2}$ and $\eta^{SOFC}_{conc,O_2}$) can be determined as described in the subsequent section.

### 2.3. Concentration overpotentials

In this section, the procedures to calculate the important concentration overpotentials of RSOFC-H in the SOSE mode are developed. The concentration overpotentials represent the resistance of the porous electrode to the transport of gaseous species [13]. According to their definitions, the concentration overpotentials of an RSOFC-H in the SOSE mode can be written as:

$$\eta^{SOSE}_{conc,H_2} = \frac{RT}{2F} \ln\left(\frac{P^{I}_{H_2}}{P^{0}_{H_2}}\right) \quad (3)$$

and

$$\eta^{SOSE}_{conc,O_2} = \frac{RT}{2F} \ln\left(\frac{(P^{I}_{O_2})^{1/2} P^{0}_{H_2O}}{(P^{0}_{O_2})^{1/2} P^{I}_{H_2O}}\right) \quad (4)$$

where $P^{I}_{H_2}$, $P^{I}_{O_2}$, and $P^{I}_{H_2O}$ represent pressure of hydrogen at the hydrogen electrode–electrolyte interface, partial pressure of oxygen at the oxygen electrode–electrolyte interface, and partial pressure of steam at the oxygen electrode–electrolyte interface, respectively; $F$ is the Faraday constant; $R$ is the ideal gas constant; the superscript 0 represents the surface of an electrode.

In a steady state, the transport of each participating component is determined by the local conservation of mass [14].

$$\nabla N_i = 0 \quad (5)$$

where $N_i$ is the mass transfer of species $i$. $H_2$ is the only component present in the porous hydrogen electrode. The transport of $H_2$ by means of permeation can be determined with Darcy's law [15,16].

$$N_{H_2} = -\frac{P_{H_2} B_g}{RT\mu_{H_2}} \nabla P_{H_2} \quad (6)$$

where $\mu_{H_2}$ is the dynamic viscosity of $H_2$ and $B_g$ is the permeation coefficient, which can be determined by a sixth-order polynomial function developed by Todd and Young [17] and the Kozeny–Carman relationship [15], respectively.

Substituting Eq. (6) into Eq. (5), the controlling equation for $H_2$ permeation in the porous hydrogen electrode can be obtained.

$$\frac{\partial}{\partial x}\left[\frac{P_{H_2} B_g}{RT\mu_{H_2}} \frac{\partial P_{H_2}}{\partial x}\right] = 0 \quad (7)$$

where $x$ is the normal distance measured from the electrode surface and is applicable to both hydrogen electrode and oxygen electrode.

At the interface of the hydrogen electrode and the electrolyte ($x = d_{H_2}$, the thickness of the hydrogen electrode), the rate of $H_2$ transport to the surface of the hydrogen electrode is equal to the $H_2$ production rate under steady state conditions. This boundary condition can be written in terms of the electrical current density $J$ as:

$$-\frac{J}{2F} = -\frac{P_{H_2} B_g}{RT\mu_{H_2}} \frac{\partial P_{H_2}}{\partial x}\bigg|_{x=d_{H_2}} \quad (8)$$

The Dirichlet boundary condition can be applied at the surface of the hydrogen electrode:

$$P_{H_2}\big|_{x=0} = P^{0}_{H_2} \quad (9)$$

Solving Eq. (7) with boundary conditions expressed in Eqs. (8) and (9), the pressure of $H_2$ at the interface of the hydrogen electrode and the electrolyte can be obtained:

$$P^{I}_{H_2} = \sqrt{(P^{0}_{H_2})^2 + \frac{JRT\mu_{H_2} d_{H_2}}{FB_g}} \quad (10)$$

Substituting Eq. (10) into Eq. (3), the concentration overpotential of the hydrogen electrode can be expressed as:

$$\eta^{SOSE}_{conc,H_2} = \frac{RT}{2F} \ln\left(\frac{\sqrt{(P^{0}_{H_2})^2 + (JRT\mu_{H_2} d_{H_2}/FB_g)}}{P^{0}_{H_2}}\right) \quad (11)$$

At the oxygen electrode side, the mass transfer phenomena become more complex as both diffusion driven by concentration gradient and permeation driven by pressure gradient occur simultaneously. The dusty gas model (DGM) is employed to describe the mass transfer within the porous oxygen electrode. Considering both diffusion and permeation, the DGM can be written as [18].

$$\frac{N_i}{D^{eff}_{i,k}} + \sum_{j=1, j\neq i}^{n} \frac{y_j N_i - y_i N_j}{D^{eff}_{ij}} = -\frac{1}{RT}\left[P\frac{dy_i}{dx} + y_i \frac{dP}{dx}\left(1 + \frac{B_g P}{D^{eff}_{i,k}\mu_m}\right)\right] \quad (12)$$

where $D^{eff}_{i,k}$ is the effective Knudsen diffusion coefficient of species $i$; $D^{eff}_{ij}$ represents the effective binary diffusion coefficient of species $i$ and $j$; $y_i$ represents molar fraction of species $i$; $P$ is the local total pressure in the oxygen electrode; and $\mu_m$

is the dynamic viscosity of the gas mixture ($O_2$ and $H_2O$). The procedure for determination of molecular diffusion and Knudsen diffusion coefficients can be found in literature [12]. The gas mixture viscosity ($\mu_m$) can be obtained by Wilke's method [19].

The above DGM can be solved numerically. The DGM domain is discretinized for the finite difference method (FDM) and an iterative approach with considerable sub-relaxation is employed to obtain the distribution of gas composition and total pressure. Computation is repeated until convergence is attained. Substituting the calculated partial pressures of $O_2$ and $H_2O$ at the interface of the oxygen electrode and the electrolyte into Eq. (4), the concentration overpotential at the oxygen electrode side can be obtained.

## 3. Results and discussion

### 3.1. Model evaluation and temperature effect

The above model has been derived to determine the *J–V* characteristics of an RSOFC-H performing dual functions of fuel cell and electrolyzer. The model evaluation for SOFC mode was provided in a previous study. In this study, the newly developed model for the SOSE mode will be evaluated by comparing the modeling results with experimental data. In the literature, only Iwahara's group [7,9,10] reported the detailed *J–V* characteristics of hydrogen production by proton-conducting based SOSE and thus their experimental data were used for model evaluation. In these experiments, the *J–V* characteristics of an electrolyte-supported SOSE cell were measured. The electrolyte, hydrogen electrode, and oxygen electrode were made of $SrCe_{0.9}Y_{0.1}O_{3-\alpha}$, Pt and $Pt + La_{0.4}Sr_{0.6}CoO_{3-\alpha}$ with thicknesses of about 500 μm, 50 μm, and 50 μm, respectively. The *J–V* data were measured at temperatures of 1073 K and 1173 K and a pressure of 1 atm.

Fig. 3(a) shows the comparison between the electrochemical modeling results and the experimental data by Iwahara et al. [10]. The values of the input parameters for the modeling analysis are shown in Table 1. The SOSE potential decreases significantly with increasing temperature (from 1073 to 1173 K). This is mainly because the Ohmic overpotential decreases significantly with increasing temperature due to higher proton conductivity. It can also be seen that the simulation results generally agree with the experimental data. The relatively large discrepancy between simulation results and experimental data may be caused by inaccurate values of electrolyte resistivity used, which were measured from Iwahara et al.'s curves [7]. In addition, the exchange current densities used for calculating the activation overpotential differ significantly in the literature [11,13,20,21], which could be another source of inaccuracy. In order to better fit the experimental data, the key parameters have been changed and an additional comparison with experimental data at a temperature of 1173 K is presented in Fig. 3(b). It can be seen that an electrolyte resistivity of 2.2 Ω m yields better simulation results (Fig. 3(b)) than 2.0 Ω m (Fig. 3(a)). In addition, when the exchange current density is changed from 4000 to 200 A $m^{-2}$, the simulation results fit the experimental data even better. The findings imply that the simulation results can fit experimental

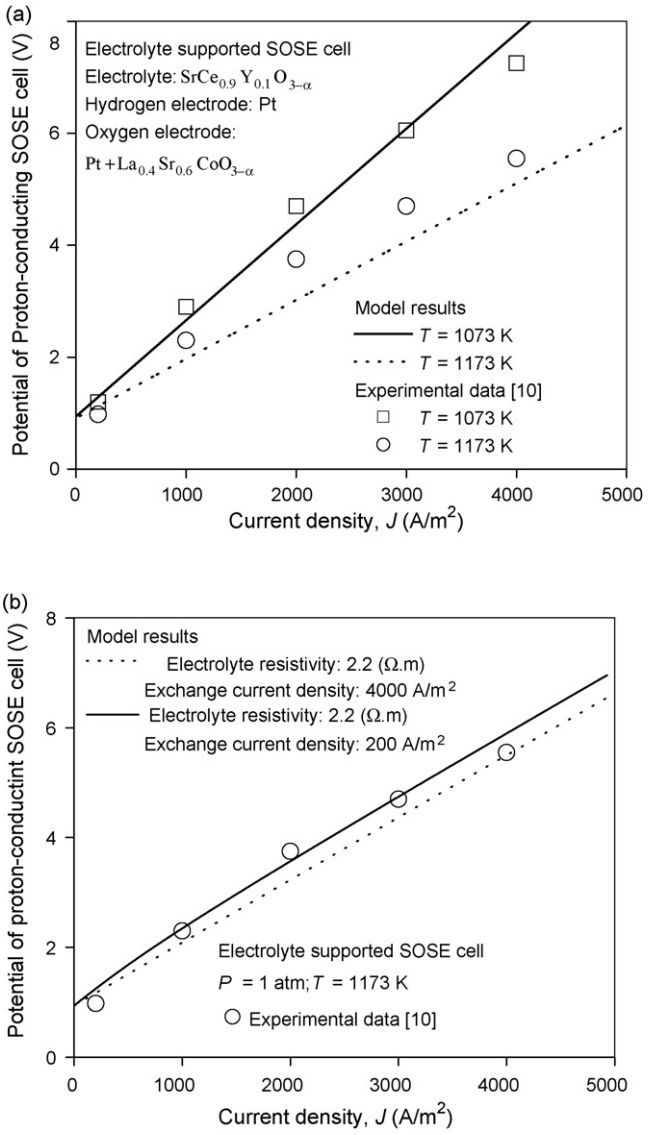


Fig. 3. Comparison between theoretical simulation results and experimental data by Iwahara et al. [10]: (a) Simulation parameters from Table 1 and (b) Different simulation parameters at 1173 K.

data well by adjusting the key parameters, such as electrolyte resistivity and exchange current density of the electrodes.

In order to better understand the characteristics of the SOSE cell for hydrogen production, the individual Ohmic, activation and concentration overpotentials were studied as shown in Fig. 4. The results show that the Ohmic overpotential dominates the activation and concentration overpotentials. At a current density of 5000A $m^{-2}$, the Ohmic overpotential is above 8 V (Fig. 4a), while both the activation and concentration overpotentials are about two to four orders of magnitude less than the Ohmic overpotential (Fig. 4b and c). This is because of (1) low ionic conductivity of the proton-conducting electrolyte and (2) thick electrolyte (i.e. 500 μm) used. The overall effect explains why the *J–V* curve approximately follows a linear relationship. The extremely high Ohmic overpotential also rules out the feasibility of electrolyte-supported configuration for RSOFC-H.

Table 1
Values of input parameters used in the present study

| Parameter | Value |
|---|---|
| Operating temperature, $T$ (K) | |
| For model evaluation | 1173 and 1073 |
| For parametric analyses | 1073 |
| Operating pressure, $P$ (atm) | 1.0 |
| Gas composition at the surface of oxygen electrode (molar ratio of $H_2O/O_2$) | 0.9/0.1 |
| Electrode porosity, $\varepsilon$ | 0.4 |
| Electrode pore radius, $r$ (μm) | 0.5 |
| Electrode tortuosity, $\xi$ | 5.0 |
| Electrolyte resistivity, $\varphi$ (Ω m) | |
| For model evaluation ($SrCe_{0.6}Y_{0.1}O_{3-\alpha}$) | 3.3 (1073 K) |
| | 2.0 (1173 K) |
| For parametric analyses ($SrCe_{0.95}Y_{0.05}O_{3-\alpha}$ or $BaCe_{0.8}Sm_{0.2}O_{2.9}$) | 1.0 |
| Electrolyte supported RSOFC-H | |
| Thickness of electrolyte, $L$ (μm) | 500 |
| Thickness of hydrogen electrode, $d_{H_2}$ (μm) | 50 |
| Thickness of oxygen electrode, $d_{O_2}$ (μm) | 50 |
| Hydrogen electrode-supported RSOFC-H | |
| Thickness of electrolyte, $L$ (μm) | 50 |
| Thickness of hydrogen electrode, $d_{H_2}$ (μm) | 500 |
| Thickness of oxygen electrode, $d_{O_2}$ (μm) | 50 |
| Oxygen electrode-supported RSOFC-H | |
| Thickness of electrolyte, $L$ (μm) | 50 |
| Thickness of hydrogen electrode, $d_{H_2}$ (μm) | 50 |
| Thickness of oxygen electrode, $d_{O_2}$ (μm) | 500 |

### 3.2. Concentration overpotentials of RSOFC-H in the SOSE mode

In practice, a cell consists of a thick layer of electrode (typically 500 μm) that can provide mechanical support, while the other electrode is a thin layer (typically 50 μm) to minimize the overpotential loss. The characteristics of different electrodes (thick or thin, hydrogen or oxygen) are shown in Fig. 5a. A thick hydrogen electrode only causes a negligible increase in the concentration overpotential in comparison with a thin hydrogen electrode. At the hydrogen electrode, the reactant ($H^+$) transporting in the solid electrolyte is not limited by the porous structure. Therefore, there is no limiting current for the hydrogen electrode. In addition, the small molecular weight of the product ($H_2$) facilitates its transport. As a result, the resistance of the porous hydrogen electrode to the gas transport is very low, leading to low concentration overpotential. For comparison, a thick oxygen electrode suffers seriously from high concentration overpotential and low limiting current density (around 4000A $m^{-2}$). Unlike the hydrogen electrode, the reactant at the oxygen electrode ($H_2O$) is transported through the pores, and, thus, its transport depends on the porous structures of the electrode. The high molecular weights of $H_2O$ and $O_2$ (product) result in low effective diffusion coefficient of $H_2O$, leading to high concentration overpotential. As a result, a hydrogen electrode-support performs better than an oxygen electrode-support in terms of low electrical energy requirement, as shown in Fig. 5b.

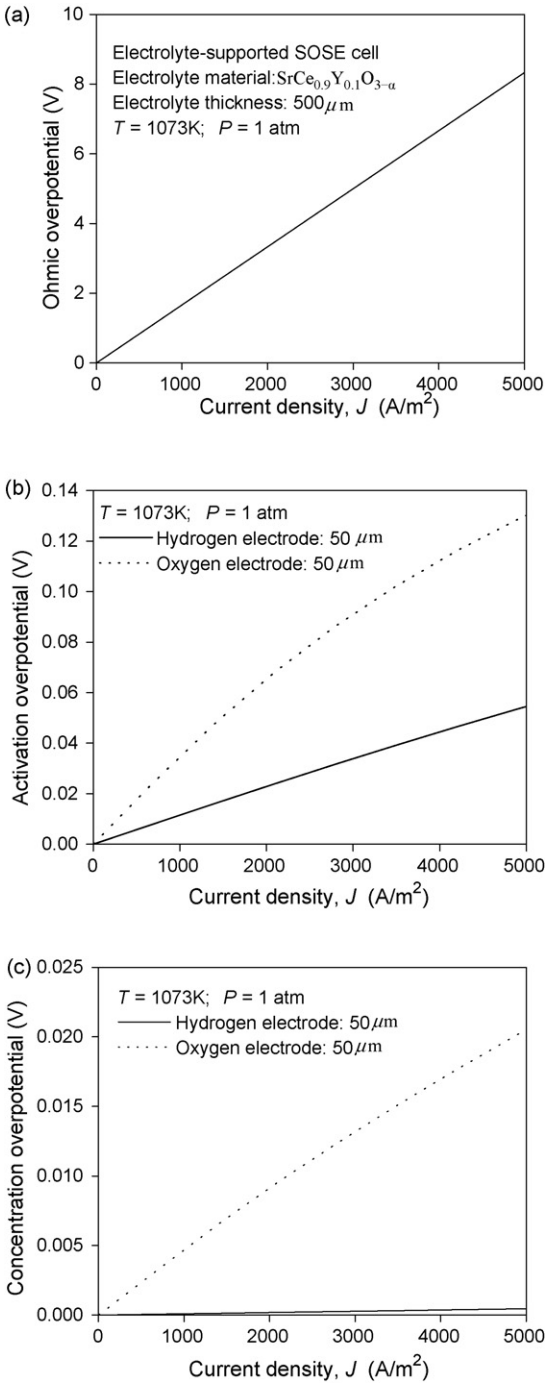


Fig. 4. Simulation results of individual Ohmic, activation, and concentration overpotentials of the electrolyte-supported SOSE cell based on proton-conducting electrolyte used by Iwahara et al. [10]: (a) Ohmic overpotential, (b) activation overpotentials, and (c) concentration overpotentials.

### 3.3. Concentration overpotentials of RSOFC-H in the SOFC mode

The concentration overpotentials of an RSOFC-H working in the SOFC mode are shown in Fig. 6a, using the electrochemical model from Ni et al. [11]. Similar to the SOSE mode, the concentration overpotentials of both thick and thin hydrogen electrodes are negligibly small. This is because the light hydrogen gas is

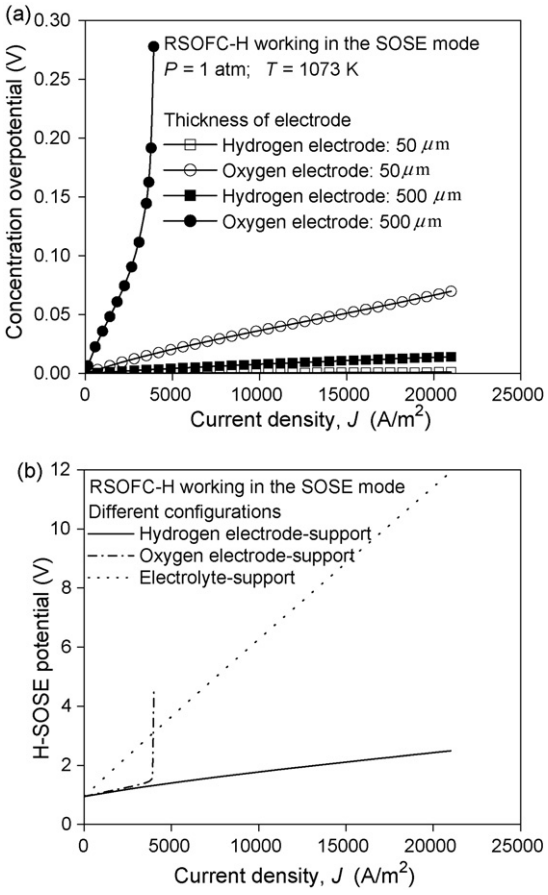


Fig. 5. Theoretical modeling results of electrochemical performance of RSOFC-H in the SOSE mode: (a) concentration overpotentials of electrodes with different thicknesses and (b) *J–V* characteristics of the cell with different support configurations.

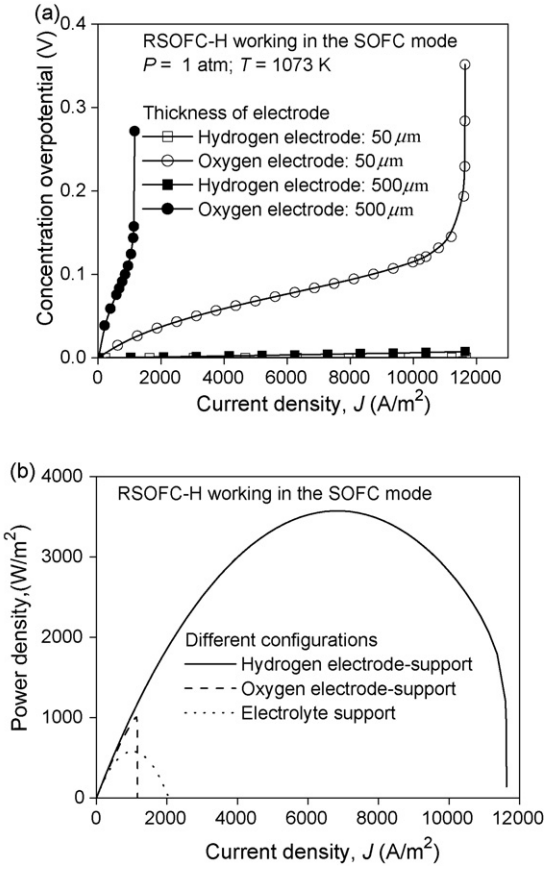


Fig. 6. Theoretical modeling results of electrochemical performance of RSOFC-H in the SOFC mode: (a) concentration overpotentials of electrodes with different thicknesses and (b) power densities of the cell with different support configurations.

transported in the hydrogen electrode quickly. Similarly, there is no limiting current density for the hydrogen electrode in the SOFC mode. For comparison, the concentration overpotentials of the oxygen electrode increase considerably when a thick electrode layer is used. It is also noted that the limiting current density of the thick oxygen electrode (500 μm) in the SOFC mode is about 1200 A m$^{-2}$, which is much smaller than that in the SOSE mode (about 4000 A m$^{-2}$). In the SOFC mode, the molecular weight of the reactant at the oxygen electrode ($O_2$) is higher than that in the SOSE mode ($H_2O$), resulting in lower rate of transport and a lower limiting current density. Due to the difference in concentration overpotentials, the hydrogen electrode-support performs better than the oxygen electrode-support in the SOFC mode, as shown in Fig. 6b.

### *3.4. Comparison between RSOFC-H and RSOFC-O and the prospect of RSOFC-H*

From the analyses in Sections 3.2 and 3.3, it can be seen that the selection of an electrode support can greatly affect the overall performance of an RSOFC. More importantly, the hydrogen electrode-support is favorable for RSOFC-H working in both SOSE and SOFC modes. For comparison, an RSOFC-O has challenges with selecting either the oxygen or hydrogen electrode as the cell mechanical support since one working mode always suffers from high concentration overpotentials. Therefore, the RSOFC-H has a natural advantage in comparison with RSOFC-O, from the cell structural design point of view.

It can also be seen from the present study that the Ohmic overpotential of RSOFC-H is yet another important source of energy loss because of low conductivity of the presently used proton conductors. Due to its high Ohmic overpotential, the proton-conducting SOFC exhibits lower maximum power density (below 0.4 W cm$^{-2}$) than the oxygen ion conducting SOFC (above 0.6 W cm$^{-2}$) [11]. In order to further enhance the performance of RSOFC-H, it is highly desirable to develop novel materials with high proton conductivity. Alternatively, fabrication of thin film electrolyte can greatly reduce the electrolyte Ohmic overpotential. In literature, the oxygen ion-conducting electrolyte of conventional RSOFC-O can be made as thin as 8 μm [22]. It is expected that the hydrogen electrode-supported RSOFC-H can be further developed to achieve high energy conversion efficiency.

## 4. Conclusions

An electrochemical model has been developed to investigate the *J–V* characteristics of an RSOFC-H based on proton-

conducting electrolyte, which can function as an SOSE to produce hydrogen fuel and as an SOFC to generate electricity using the hydrogen fuel produced. It is found that the hydrogen electrode-support is favorable for both SOSE and SOFC modes. For comparison, a conventional RSOFC-O based on oxygen ion-conducting electrolyte will cause high concentration overpotential in either one of two working modes no matter which electrode-support (hydrogen or oxygen) is selected. The natural advantage of RSOFC-H makes it a promising technology to support renewable energy utilization. The present study suggests that development work on electrolyte materials with higher proton conductivity and enhanced fabrication of thin film electrolytes can improve RSOFC performance.

## Acknowledgements

The work described in this paper was part of an ongoing project supported by a grant from the Research Grants Council of Hong Kong, PR China (HKU7150/05E) and the CRCG of the University of Hong Kong.

## References

[1] O.A. Marina, L.R. Pederson, M.C. Williams, G.W. Coffey, K.D. Meinhardt, C.D. Nguyen, E.C. Thomsen, J. Electrochem. Soc. 154 (2007) B452–B459.
[2] M. Ni, M.K.H. Leung, D.Y.C. Leung, J. Power Sources 163 (2006) 460–466.
[3] J. Guan, B. Ramamurthi, J. Ruud, J. Hong, P. Riley, D. Weng, N. Minh, DOE Hydrogen Program 2007 Annual Merit Review, May 15–18, 2007, Arlington, Virginia, U.S.A., 2007.
[4] H. Uchida, S. Watanabe, Y. Tao, N. Osada, M. Watanabe, 10th International Symposium on Solid Oxide Fuel Cells (SOFC-X), June 3–8, 2007, Nara, Japan, 2007.
[5] T. Matsui, A. Ozaki, R. Kikuchi, K. Eguchi, Proceedings of the 9th International Symposium on Solid Oxide Fuel Cells (SOFC-IX), May 15–20, 2005, Quebec city, Canada, 2005.
[6] A. Virkar, G. Tao, Proceedings of the 209th ECS meeting, May 7–12, 2006, Denver, Colorado, U.S.A., 2006.
[7] H. Iwahara, Solid State Ionics 28–30 (1988) 573–578.
[8] R.R. Peng, Y. Wu, L. Yang, Z.Q. Mao, Solid State Ionics 177 (2006) 389–393.
[9] H. Iwaraha, Y. Asakura, K. Katahira, M. Tanaka, Solid State Ionics 168 (2004) 299–310.
[10] H. Iwahara, H. Uchida, I. Yamasaki, Int. J. Hydrogen Energ. 12 (1987) 73–77.
[11] M. Ni, M.K.H. Leung, D.Y.C. Leung, Fuel Cells 7 (2007) 269–278.
[12] M. Ni, M.K.H. Leung, D.Y.C. Leung, Chem. Eng. Technol. 29 (2006) 636–642.
[13] S.H. Chan, K.A. Khor, Z.T. Xia, J. Power Sources 93 (2001) 130–140.
[14] R. Krishna, J.A. Wesselingh, Chem. Eng. Sci. 52 (1997) 861–911.
[15] J.H. Nam, D.H. Jeon, Electrochim. Acta 51 (2006) 3446–3460.
[16] M. Ni, M.K.H. Leung, D.Y.C. Leung, J. Power Sources 168 (2007) 369–378.
[17] B. Todd, J.B. Young, J. Power Sources 110 (2002) 186–200.
[18] J.W. Veldsink, G.F. Versteeg, W.P.M. Van Swaaij, R.M.J. Van Damme, Chem. Eng. J. Biochem. Eng. J. 57 (1995) 115–125.
[19] R.C. Reid, J.M. Prausnitz, B.E. Poling, The Properties of Gases & Liquids, fourth ed., McGraw-Hill Book Company, New York, 1987.
[20] E. Hernandez-Pacheco, D. Singh, P.N. Hutton, N. Patel, M.D. Mann, J. Power Sources 138 (2004) 174–186.
[21] Y.X. Lu, L. Schaefer, P.W. Li, J. Power Sources 140 (2005) 331–339.
[22] F. Zhao, A.V. Virkar, J. Power Sources 141 (2005) 79–95.